

New Challenges in Plasma Accelerators: Final Focusing for Wakefield Colliders

Keegan Downham

*University of California, Santa Barbara, CA 93106 and
SLAC National Accelerator Laboratory, Menlo Park, CA 94025*

Spencer Gessner

SLAC National Accelerator Laboratory, Menlo Park, CA 94025

Lewis Kennedy and Rogelio Tomás

CERN, Geneva, CH

Andrei Seryi

Old Dominion University, Norfolk, VA 23529

(Dated: January 31, 2026)

The focusing of particle beams for collider experiments is crucial for maximizing the luminosity and thus the discovery potential of these machines. In recent years, plasma wakefield acceleration has emerged as a leading candidate for achieving higher energy collisions with smaller facility footprints due to the large accelerating gradients in the plasma. This higher beam energy poses significant challenges for the final focusing system of the collider. Here, we discuss the various challenges of final focusing for TeV-scale plasma accelerators and propose possible solutions. Finally, we present the first design of a final focusing system for a 10 TeV linear wakefield collider, evaluate its performance, and discuss its shortcomings as well as improvements for future designs.

PACS numbers:

I. INTRODUCTION

The role of the final focusing system (FFS) in a collider is to demagnify the beams to the desired spot sizes at the interaction point (IP) in order to maximize the luminosity \mathcal{L} :

$$\mathcal{L} \propto \frac{1}{\sigma_x \sigma_y} \quad (1)$$

where σ_x and σ_y are the root-mean-square beam sizes in the x and y planes, respectively. For flat beam collisions with $\sigma_x \gg \sigma_y$, this focusing can be achieved by arranging pairs of quadrupole magnets into a telescope, which provides point-to-point and parallel-to-parallel imaging [1]. Complications arise when considering beams with a finite energy spread δ , as particles with different energies are focused to different longitudinal positions near the IP. These chromatic aberrations, if left untreated, result in an increase of the beam size at the IP and degrade the luminosity of the collider. Furthermore, the strong focusing fields of the quadrupoles closest to the IP, referred to as the final doublet (FD), induce the emission of incoherent synchrotron radiation (SR), which further increases the energy spread of the beam, known as the Oide effect. Schemes for handling the chromatic effects have been demonstrated at the SLAC Linear Collider (SLC) [2] and Final Focus Test Beam (FFTB) [3] using dedicated chromatic correction sections. A more recent

compact approach [4] relies on local chromaticity correction by utilizing sextupoles interleaved with the FD, decreasing the overall length of the FFS while providing larger FD bandwidth than the schemes with dedicated chromatic correction sections. First experimental demonstrations of this approach are being carried out at ATF2 [5–8]. In general, the FFS designs for future colliders need further experimental demonstrations in terms of operational reproducibility, and achieved bunch charge and IP parameters [9]. A dedicated comparison of FFS designs with the traditional and the compact approaches is presented in reference [10].

Plasma wakefield acceleration (PWFA) [11] has emerged as a leading candidate for achieving compact, multi-TeV scale colliders due to the high acceleration gradients with respect to state-of-the-art metallic superconducting radio-frequency (SRF) technology [12, 13]. The drastic length reduction of the plasma linac may lead to a situation where the beam delivery system (BDS), which includes the FFS, becomes the largest contribution to the facility footprint. The scaling of the BDS system for multi-TeV colliders was examined in ref. [14]. In the FFS design with the local compact chromatic correction scheme, the length of the FFS scales approximately as [4]:

$$L_{\text{FFS}} \propto E^{7/10}, \quad (2)$$

where E is the energy of the particles. Another scheme,

derived for scaling the LHC interaction region to FCC-hh beam energies under the assumption of a constant beam stay clear, utilizes a different scaling [15]:

$$L_{\text{FFS}} \propto E^{1/3} \quad (3)$$

A similar procedure was also utilized for scaling the CLIC 3 TeV FFS to the 7 TeV design [16, 17]. The optimal scaling for the FFS length with energy is expected to fall somewhere between those shown in Eq. 2 and Eq. 3 by allowing some luminosity loss due to synchrotron radiation. As a result, higher energy colliders will require a longer (and thus more expensive) FFS. Compact, high-energy linear colliders must balance luminosity and length considerations for the FFS.

The desire for high intensity electron beams at future PWFA colliders also poses a problem for the achievable luminosity. Particles in colliding beams interact strongly with the field produced by the opposing beam, resulting in the emission of SR. This process, known as beamstrahlung, causes each beam to radiate away its energy and reduce the center-of-mass energy of the colliding particles, broadening the luminosity spectrum [18].

In the following sections we discuss each of these challenges in more detail and propose possible solutions. Finally, we present the first design of a FFS as part of the 10 TeV Wakefield Collider Design Study [19] and assess its performance in the context of a future PWFA collider design.

II. BEAM SIZE LIMITING PROCESSES

In this section, we review the physical processes that limit our ability to focus beams to arbitrarily small spot sizes. These processes include limitations of beam transport systems as well as dynamic radiative effects.

A. Chromatic Effects

In practice, all particle beams have some finite energy spread, δ . The bending of an individual particle in a magnetic field depends on the energy of the particle itself, and, due to this, particles of different energies are focused differently in a quadrupole field. This is illustrated in Figure 1 for particles with an energy offset Δp with respect to the nominal particle energy p_0 ; the particles are focused to different points along the longitudinal coordinate, which increases the spot size at the focal point for the reference particle energy (the IP).

Typically, the largest focusing gradients in the FFS are present in the final doublet (FD), which demagnify the beams at the IP to maximize the luminosity. As a result,

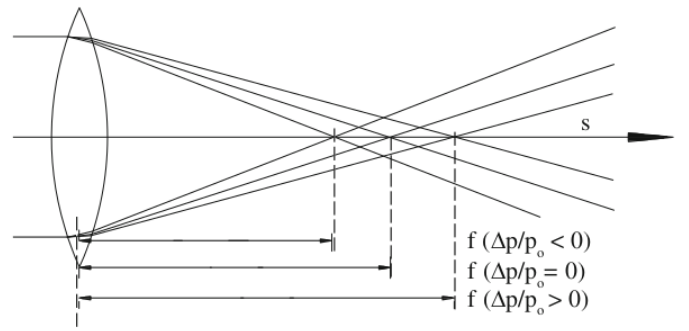


FIG. 1: Diagram illustrating the focal points for particles with momentum deviations with respect to the nominal reference energy p_0 . Figure adapted from Ref. [20].

the largest contribution to the spot size growth due to chromaticity comes from the FD. To lowest order, the spot size at the IP for a beam with finite relative energy deviation δ can be written as, e.g. [21]:

$$\sigma_i^* = \sqrt{\epsilon_i \beta_i^* (1 + \xi_i^2 \delta^2) + D_i^2 \delta^2} \quad (4)$$

where ϵ_i is the geometric emittance for the coordinate i , β_i^* is the beta function for coordinate i , D_i is the dispersion, and ξ_i is the chromaticity. At the IP, design D_i is typically zero and an expression for ξ_i is given in Section III B.

Chromatic effects generated by the FD can be compensated by a combination of bending magnets to generate dispersion and sextupoles to provide transverse-position-dependent kicks. Two main approaches for chromatic correction have emerged for linear colliders, differing in the arrangement of the bending sections and sextupoles. The first scheme developed [2, 3] utilized dedicated sections for cancelling the vertical and horizontal chromaticity, each comprised of bending magnets with pairs of sextupoles; the sections themselves were placed in regions of high dispersion and large- β . To cancel the geometric aberrations generated by the sextupoles, the sextupole pairs are arranged such that they are separated by a minus identity transfer matrix. A different scheme [4] relies on local chromaticity correction by placing sextupoles just before and between the FD quadrupoles with a long upstream bending section to generate the necessary dispersion. Horizontal second-order dispersion is introduced by the sextupoles, and is corrected by designing the optics such that half of the total horizontal chromaticity is generated upstream of the FD. Another pair of sextupoles, placed before the bending section, are utilized to cancel the geometric aberrations, provided that they have the opposite phase of the FD sextupoles.

B. Oide Effect

The strong focusing fields of the FD quadrupoles acting on the beam cause the emission of hard SR near the IP, resulting in emittance growth of the beam and therefore increasing the beam spot size [22]. With SR emission, the spot size at the IP for a linear collider is given by:

$$\sigma_y^{*2} = \beta_y^* \epsilon_y + \frac{110}{3\sqrt{6\pi}} r_e \lambda_e \gamma^5 F(\sqrt{K}L, \sqrt{K}\ell^*) \left(\frac{\epsilon_y}{\beta_y^*} \right)^{5/2} \quad (5)$$

where r_e is the classical electron radius, λ_e is the Compton wavelength, γ is the Lorentz factor, and F is a dimensionless function given by:

$$F(\sqrt{K}L, \sqrt{K}\ell^*) = \int_0^{\sqrt{K}L} |\sin \phi + \sqrt{K}\ell^* \cos \phi|^3 \times \left[\int_0^\phi (\sin \phi' + \sqrt{K}\ell^* \cos \phi') \right]^2 d\phi \quad (6)$$

where K is the focusing gradient of the quadrupole, L is the thickness of the quadrupole, and ℓ^* is the distance between the front of the quadrupole and the IP. A generalization of the Oide effect considering the two transverse dimensions is presented in [23] showing a more pronounced growth with the vertical emittance and a dependence of quadratic order on the horizontal emittance. The function in Equation 5 has a minimum when β_y^* is

$$\beta_y^* = \left[\frac{275}{3\sqrt{6\pi}} r_e \lambda_e F(\sqrt{K}L, \sqrt{K}\ell^*) \right]^{2/7} \gamma (\epsilon_{Ny})^{3/7} \quad (7)$$

This minimum spot size at the IP, referred to as the Oide limit, is given by the following expression,

$$\sigma_y^* = \left(\frac{7}{5} \right)^{1/2} \left[\frac{275}{3\sqrt{6\pi}} r_e \lambda_e F(\sqrt{K}L, \sqrt{K}\ell^*) \right]^{1/7} (\epsilon_{Ny})^{5/7} \quad (8)$$

While the Oide limit has not been directly measured at collider experiments, it is a fundamental ingredient in the design of future proposed colliders, e.g. [24]. Possible solutions to reduce the impact of the Oide effect involve increasing the length or decreasing the gradient of the final quadrupole [25], and utilizing a pair of octupole magnets before and after the final quadrupole [26]. It has also been shown that the use of adiabatic plasma lenses [27] may mitigate the Oide effect. Further discussion of plasma lenses is presented in Section IV A.

C. Beamstrahlung

Near the IP, each beam interacts with the electromagnetic field produced by the other beam, causing energy

to be radiated away in the form of SR. This increases the energy spread of each beam, allowing for collisions at lower-than-nominal energy and resulting in a deterioration of the luminosity while also providing additional background in the detector. The field strength of the beam, which characterizes the level of beamstrahlung, is represented by the dimensionless parameter Υ . For Gaussian beams:

$$\Upsilon = \frac{5\gamma N_b r_e^2}{6\sigma_z (\sigma_x + \sigma_y) \alpha} \quad (9)$$

where N_b is the bunch population, r_e is the classical electron radius, σ_z is the RMS bunch length, and $\alpha \approx 1/137$ is the fine structure constant.

For a fixed beam size at the IP, the problem of beamstrahlung can be greatly reduced by the use of flat beams, whereby $\sigma_x \gg \sigma_y$. The plasma-based collider designs with collision energy $\sqrt{s} > 1$ TeV operate in the so-called quantum beamstrahlung regime ($\Upsilon \gg 1$) due to the high collision energy and short bunch lengths. In this regime, for fixed luminosity, beam energy, and beam sizes at the IP, the number of photons emitted per lepton n_γ and energy spread resulting from beamstrahlung δ_γ scale as [28]:

$$n_\gamma \propto \sigma_z^{1/3} \Upsilon^{2/3} \quad (10)$$

and

$$\delta_\gamma \propto \sigma_z^{1/3} \Upsilon^{2/3}. \quad (11)$$

Equations 10 and 11 suggest that shorter bunch lengths help to reduce deleterious beamstrahlung effects. New studies have examined beamstrahlung as an inevitable aspect of collisions at 10 TeV and explore the physics reach of machines with broad luminosity spectra [28–30].

III. STUDIES AT 10 TEV

A nominal flat-beam FFS design for parton center-of-mass (pCM) energies of 10 TeV is presented here as part of the 10 TeV Wakefield Collider Design Initiative [19]. This design is extrapolated from the 7 TeV FFS for the Compact Linear Collider (CLIC) [17], which employs the local chromaticity correction scheme.

A. Scaling CLIC Lattice to 10 TeV

The increased beam energy of 10 TeV with respect to the CLIC FFS design energy of 7 TeV necessitates an energy-dependent scaling to account for the change in beam rigidity and the impact of SR on the luminosity.

A procedure, outlined in Ref. [15], is performed on the CLIC 7 TeV FFS lattice and summarized as follows: the length scales and normalized magnet strengths are scaled according to a scaling factor κ related to the ratio of the nominal and new beam energies:

$$\kappa = \left(\frac{10 \text{ TeV}}{7 \text{ TeV}} \right)^{1/3} \approx 1.126 \quad (12)$$

The scaling factor is applied for each power of the length in the relevant quantities, as shown in Table I. This scaling is taken as a starting point for a FFS design at 10 TeV; future optimizations of the FFS to achieve the desired spot sizes at the IP and maximize the luminosity at 10 TeV will likely require further length scalings of the FFS elements beyond what is described above.

Scalings of relevant parameters			
Quantity	Units	Pre-scaling	Post-scaling
Beta Function	[m]	β	$\kappa\beta$
Magnet and Drift Lengths	[m]	ℓ	$\kappa\ell$
Norm. Dipole strength	[m ⁻¹]	k_0	$\kappa^{-1}k_0$
Norm. Quadrupole strength	[m ⁻²]	k_1	$\kappa^{-2}k_1$
Norm. Sextupole strength	[m ⁻³]	k_2	$\kappa^{-3}k_2$

TABLE I: Scaling of parameters for increased FFS design energy. The value of the parameter κ is given by Eq. 12.

Under this scheme, the overall length of the FFS increases from 767.671 m at 7 TeV to 864.588 m at 10 TeV. This procedure ensures a constant beam stay clear while maintaining the same normalized emittances, resulting in the shortest possible interaction region length. The parameters for the 7 TeV and 10 TeV FFS designs are summarized in Table II. Figure 2 shows the β functions and dispersions for the 7 TeV and 10 TeV FFS designs; the scaling procedure results in a mild increase in the beta functions at the IP. However, for fixed normalized emittance $\epsilon_{i,N}$, the increased beam energy results in a decrease in the geometric emittance, commonly referred to as adiabatic damping:

$$\epsilon_i = \frac{\epsilon_{i,N}}{\beta\gamma} \quad (13)$$

7 TeV and 10 TeV FFS Parameters		
Parameter	7 TeV	10 TeV
Length [m]	767.671	864.588
L^* [m]	6	6.757
β_x^*/β_y^* [mm]	7.00/0.16	7.88/0.18
ϵ_x/ϵ_y [nm]	660/20	660/20
σ_x^*/σ_y^* [nm]	34.44/1.55	32.40/2.31
$\sigma_{x,SR}^*/\sigma_{y,SR}^*$ [nm]	40.67/3.02	43.02/4.21
$\delta_{p,rms}$ [%]	0.3	0.3

TABLE II: Parameters for the 7 TeV and 10 TeV FFS designs.

where here $\beta = \frac{v}{c}$ is the longitudinal velocity normalized to the speed of light. Due to the reduction in geometric emittance, to first order (in the absence of dispersion), the beam size after scaling $\tilde{\sigma}_i$ is approximately reduced by a factor of κ :

$$\tilde{\sigma}_i = \sqrt{\frac{\epsilon_{i,N}\tilde{\beta}_i}{\tilde{\beta}\tilde{\gamma}}} \approx \sqrt{\frac{\epsilon_{i,N}(\kappa\beta_i)}{(\kappa^3\beta\gamma)}} = \frac{1}{\kappa}\sigma_i \quad (14)$$

Consequently, the geometric luminosity should then increase approximately by a factor of κ^2 .

B. Lattice Performance

In reality, the beam size at the IP is comprised of various terms at different orders in the transfer map expansion. The transfer map X relates the transverse particle coordinates z_f at a point along a beamline to the initial coordinates $(x_i, p_{x,i}, y_i, p_{y,i}, \delta_i)$ [31]:

$$z_f = \sum_{jklmn} X_{z,jklmn} x_i^j p_{x,i}^k y_i^l p_{y,i}^m \delta_i^n, \quad (15)$$

where $X_{z,jklmn}$ are the map coefficients for the particular final coordinate. The order of the map, M , is the largest sum of the powers among the considered terms:

$$M = j + k + l + m + n. \quad (16)$$

The IP vertical chromaticity ξ_y can be expressed in terms of the map coefficients as [21]

$$\xi_y^2 = \frac{1}{\beta_y^*} \left(X_{y,00101}^2 \beta_{y0} + \frac{X_{y,00011}^2}{\beta_{y0}} \right), \quad (17)$$

where β_y^* is the vertical IP beta function and β_{y0} is the beta function at the start of the FFS. Above $M = 2$, calculation of map coefficients is analytically challenging, however many modern particle tracking codes (such as MAD-X [32] with the Polymorphic Tracking Code [33]) can numerically calculate the coefficients for arbitrary M . The spot size at a given M is a complicated function of the map coefficients, and can be calculated using the MAPCLASS2 [34] program interfaced with MAD-X [32] or the Polymorphic Tracking Code (PTC) [33]. For the 10 TeV FFS design, the spot size calculated as a function of the map order is shown in Figure 5 up to $M = 5$. The values are compared with the spot sizes obtained with the particle tracking code PLACET [35] and exhibit good agreement. To evaluate the luminosity with various beam-beam effects included, the particle coordinates from tracking are fed into GuineaPIG [36]. The luminosity is calculated with and without SR enabled in PLACET, and the results are shown in Table III. The

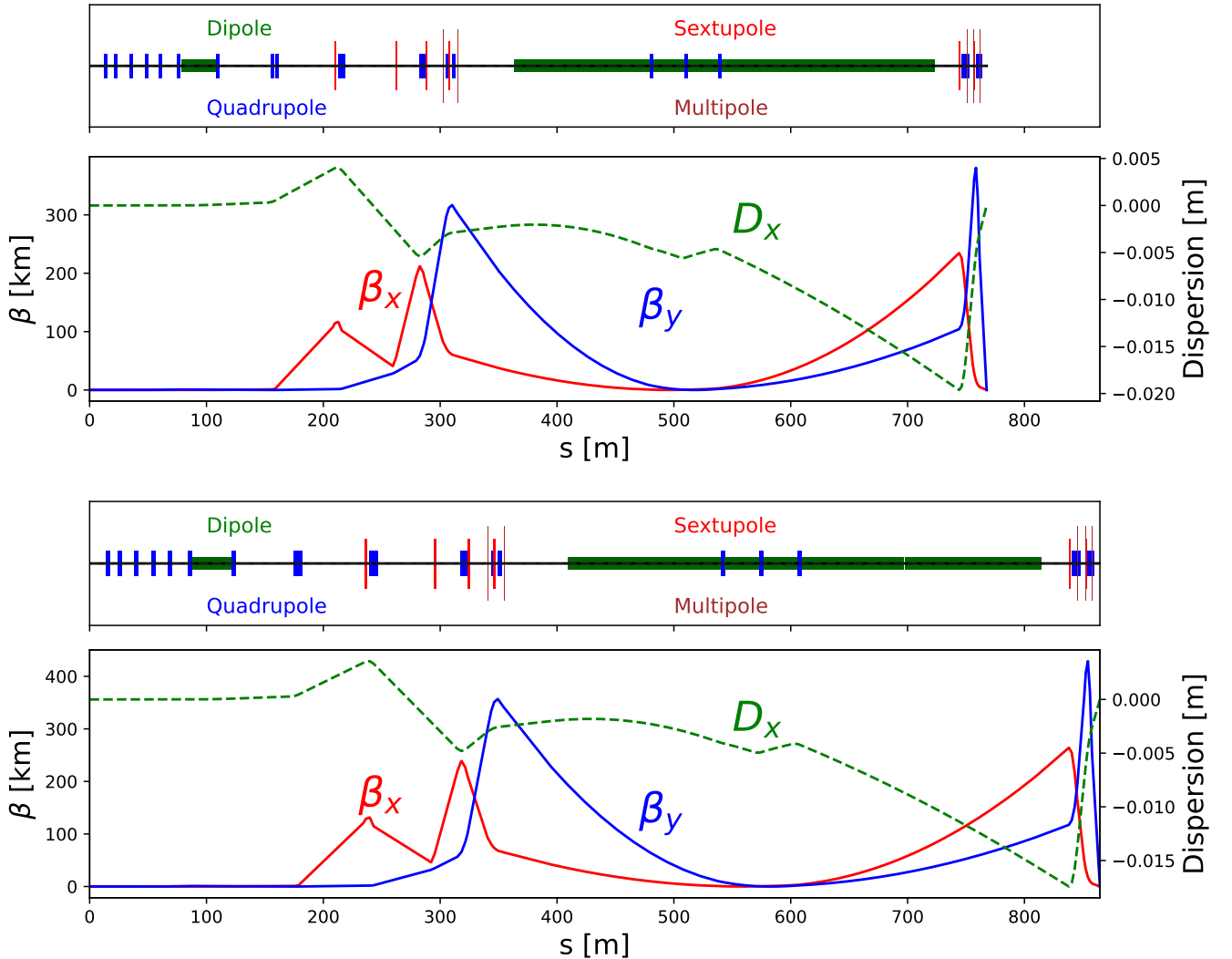


FIG. 2: Horizontal and vertical β functions and dispersion for the 7 TeV (top) and 10 TeV (bottom) FFS. Surveys of the FFS designs are shown above each plot using the same horizontal scale. The 7 TeV design is 767 meters long and the 10 TeV design is 865 meters long. Dipoles shown in green, quadrupoles in blue, sextupoles in red, and higher-order multipoles shown in brown.

impact of SR is rather considerable, increasing the beam size in the vertical direction by a factor of ≈ 2 and in the horizontal direction by a factor of ≈ 1.25 .

The sensitivity of the chosen parameters to the Oide limit was considered as well. At fixed β_y^* , the vertical emittance was scanned for different values of the horizontal emittance, as shown in Figure 3. The values for the 10 TeV FFS, denoted by the black dot, is in a region where the Oide effect starts to become significant, as the slope of the red curve at this point falls between the spot size scaling predicted by Equation 14 (purple line) and Equation 8 (blue line). This behavior is also apparent when varying β_y^* for fixed emittances. Figure 4 shows the evolution of the vertical beam size at the IP (purple curve) and luminosity (red curve) for different β_y^* values.

As indicated by the teal line, the β_y^* chosen for the 10 TeV FFS maximizes the luminosity, while the minimum σ_y^* is achieved for a β_y^* that is ≈ 4 times larger. This increase in the beam size at peak luminosity results from the fact that the beam size is sensitive to tails in the beam that are generated by higher-order aberrations and SR from quadrupoles (e.g. Oide effect), while the luminosity is highly dependent on the core of the beam distribution.

IV. TAKEAWAYS AND FUTURE STUDIES

The 10 TeV FFS lattice presented here is the first design of a FFS design for a linear collider operating at a parton center of mass energy of 10 TeV. However, there

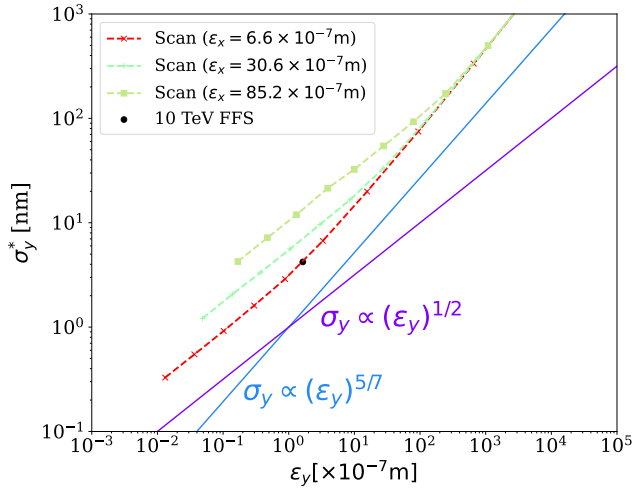


FIG. 3: Vertical beam size at the IP as a function of the normalized vertical emittance. Green and red curves show beam size for different values of the normalized horizontal emittance, while the blue and purple lines shown the expected beam size scaling with (Eq. 8) and without (Eq. 14) the Oide effect, respectively. Beam sizes are calculated using PLACET.

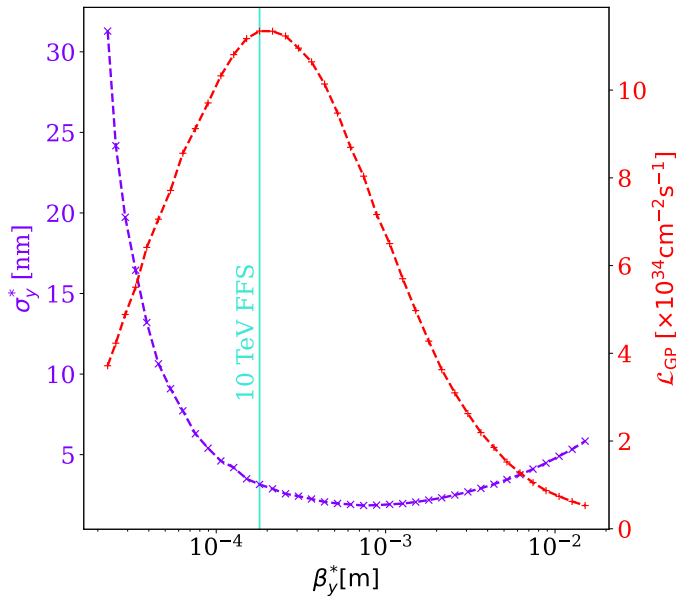


FIG. 4: Vertical beam size (purple) and luminosity (red) at the IP as a function of the vertical beta function at the IP. The vertical line shows the nominal beam size for the 10 TeV FFS design. Values for β_y^* obtained from MAD-X, while spot sizes and luminosity obtained via PLACET simulations and GuineaPIG, respectively.

	σ_x^* [nm]	σ_y^* [nm]	\mathcal{L}_{GP} [$10^{34} \text{cm}^{-2} \text{s}^{-1}$]
Without SR	32.40	2.31	19.2
With SR	43.02	4.21	10.8
Target Values	18.4	0.45	34.1

TABLE III: Beam size and Luminosity for the 10 TeV FFS with and without synchrotron radiation enabled and comparison with idealized target values adapted from Ref. [28]. Spot sizes calculated using PLACET and Luminosity calculated using GuineaPIG.

are various improvements that can be made to maximize its performance. The increase in the vertical and horizontal beam sizes due to SR can be reduced by increasing the lengths and decreasing the gradients of the final focusing quadrupoles. Additionally, the contribution to the horizontal spot size growth from SR in the bending sections may be reduced by increasing the lengths or decreasing the bending angles of the dipoles, with corresponding adjustments to the sextupole strengths to maintain small horizontal dispersion at the IP. To investigate this, a bending factor was introduced as a multiplier to the dipole strength and the inverse of the sextupole strength. Figure 6 shows the spot sizes (top) and luminosity (bottom) as a function of this bending factor, with a maximum luminosity and minimum IP spot size occurring at the nominal value. This suggests possible higher-order aberrations contributing to the decrease in luminosity, requiring careful study of the higher-order optics to mitigate these effects.

In the context of the 10 TeV wakefield collider design study [19], this first 10 TeV FFS design falls short of the luminosity target of $\mathcal{L} = 34.1 \times 10^{34} \text{cm}^{-2} \text{s}^{-1}$ for a flat-beam PWFA collider outlined by the Snowmass 2021 report [28]. Adjusted to 10 TeV from the initial 15 TeV proposed design energy for a flat-beam PWFA collider, the target beam sizes in the vertical and horizontal directions are 0.45 nm and 18.4 nm, respectively; a factor of ≈ 10 smaller in y and ≈ 2.5 smaller in x. It should be noted that these reported target values were computed without any consideration for realistic beam dynamics and thus represent an idealized scenario. Even with the proposed improvements stated above, to achieve this decrease in the beam size, a more dedicated redesign of the lattice is likely required.

Planned future studies include the design of a round-beam FFS at 10 TeV, leveraging the fact that PWFA is easier to achieve with round beams. For this, two designs will be considered: one consisting of conventional focusing elements while the other incorporating plasma lenses into the FFS to attempt to reduce its overall length and improve focusing capabilities. A discussion on the properties of plasma lenses is presented in Section IV A.

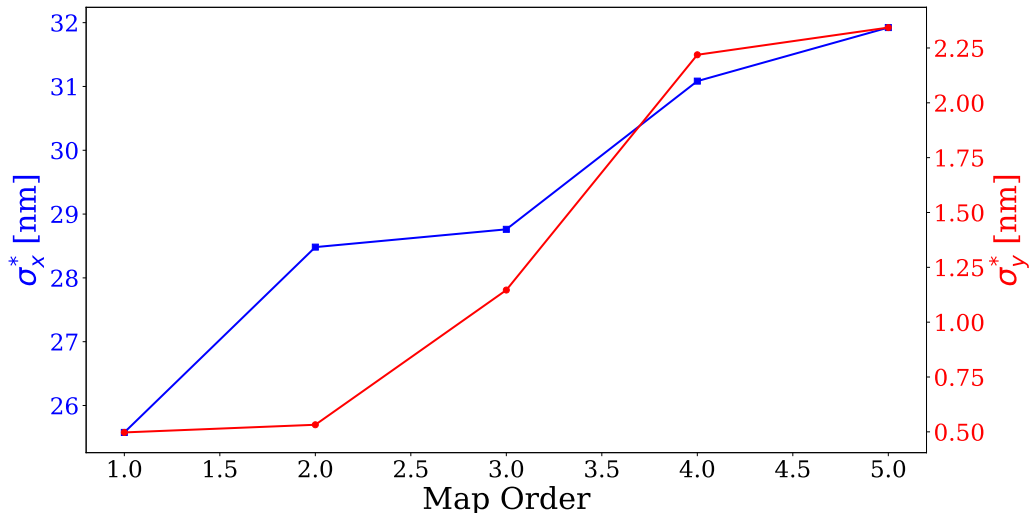


FIG. 5: Horizontal (blue) and vertical (red) beam sizes at 10 TeV calculated to different orders in the map. Values calculated using MAPCLASS2.

Finally, we should note that the traditional Beam Delivery System (BDS) in conventional linear collider designs includes several additional subsystems beyond the Final Focus and diagnostic sections. These include the beam switch yard (for dual interaction points or tune-up beam dump beamlines) and, most notably, the energy and betatron collimation sections.

The characteristics and length of the collimation sections depend on various design decisions and assumptions, such as the use of survivable versus consumable spoilers, the expected fractional beam population in the transverse and energy tails, and many other factors. As seen in earlier BDS designs—such as that of CLIC—at energies above 1 TeV, the collimation system can become the dominant component in terms of length. This occurs because, under typical design assumptions, its scaling with energy is less favorable than that of the final focus system itself.

Consequently, for a 1-10 TeV center-of-mass plasma-based linear collider to remain competitive, the design assumptions for the collimation system must be fundamentally reconsidered. Future design work on collimation optimized for plasma colliders will include, but not be limited to, concepts such as distributed collimation integrated within the plasma acceleration sections, modified approaches to protecting the experimental detector from backgrounds, and related ideas. The development of an optimized collimation system will be an important component of our future studies.

A. Plasma Lenses

The thin, underdense, passive plasma lens [37] is a promising alternative to conventional quadrupole magnets for focusing particle beams. Unlike quadrupoles, plasma lenses can provide axisymmetric, geometric-aberration-free focusing, allowing for pairs of quadrupoles to be replaced by a single plasma lens. In addition, plasma lenses can achieve focusing gradients many orders of magnitude larger than those achieved by quadrupoles. For a thin plasma lens of non-uniform number density $n_0(z)$, the focal length is given by the following expression [37]:

$$f = \frac{1}{KL} = \frac{1}{2\pi r_e} \frac{\gamma}{\int n_0(z) dz} \quad (18)$$

A comparison of the focal lengths for a plasma lens of density $n_0 = 10^{17} \text{cm}^{-3}$ and quadrupole magnets for a 5 TeV electron beam is presented in Table IV. These properties of the plasma lens are highly attractive, as they are useful for reducing the overall length of the FFS while providing smaller beam spot sizes at the IP.

A particularly useful application of the plasma lens in the FFS of a TeV-scale collider would be the replacement of quadrupole pairs (such as the FD) in order to shrink the overall length needed for the FFS [38]. Although plasma lenses offer high focusing gradients, the hard SR emission (Oide effect) can be avoided by shaping the lens such that it acts as an adiabatic focuser [27]. This provides a great advantage over conventional quadrupole focusing near the IP as it allows for smaller achievable

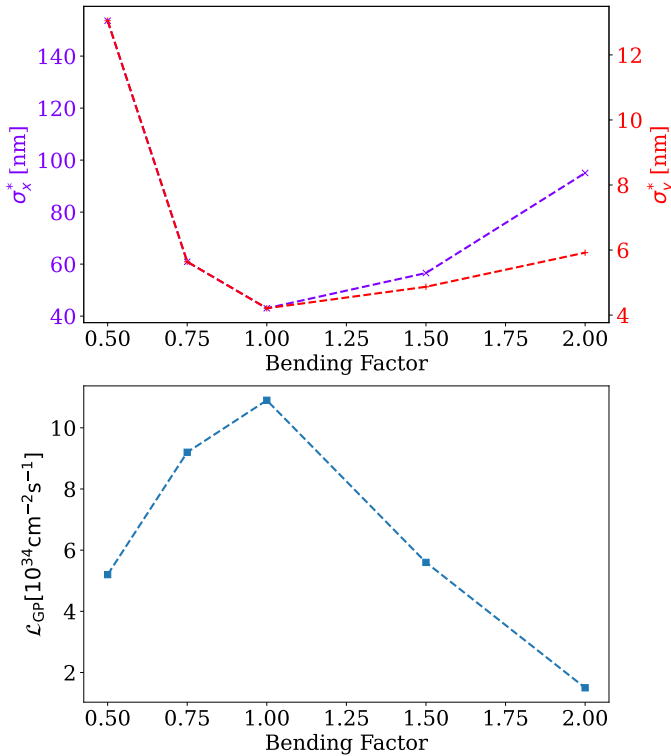


FIG. 6: Beam sizes (top) and luminosity (bottom) for different values of the bending factor. Values for the spot sizes and luminosity were obtained via PLACET simulations and GuineaPIG, respectively.

spot sizes. Furthermore, in the adiabatic regime, the focusing provided by plasma lenses is achromatic; particles of different energies are focused to the same point. Consequently, this property could alleviate the need for chromatic correction in the FFS and reduce the overall length by eliminating the need for long bending sections and sextupoles.

Despite their numerous advantages over conventional focusing elements, plasma lenses do pose significant chal-

lenges to implement in future colliders. Precise shaping of the plasma lens to achieve adiabatic focusing is difficult to achieve in practice, and this remains an active field of research. For colliders with high repetition rates (kHz or above), plasma lenses may create concerns as to their robustness, as the plasma recovery time may result in density profile variations on a shot-to-shot basis, leading to different focusing properties. It has also been demonstrated that the driving of plasmas using flat beams can lead to asymmetric focusing fields experienced by the witness bunch and variation in the focusing fields along the longitudinal coordinate [39], necessitating precise experimental control and matching to prevent chromatic beam size growth and proper focusing along both axes. Additionally, the desire for adiabatic focusing would increase the plasma density closer to the IP, resulting in beam-plasma scattering that could result in emittance growth [27] and background events in the detector [38]. Finally, despite successful experimental demonstrations of plasma lensing of positron beams [40], it remains an open question as to whether or not positrons can be focused to small spot sizes using a plasma lens without geometric aberrations [41].

V. CONCLUSIONS

We present the first design of a 10 TeV final focusing system by scaling up the version utilized for CLIC 7 TeV, resulting in a luminosity of $1.08 \times 10^{35} \text{ cm}^{-2} \text{ s}^{-1}$. The reduction to the luminosity due to synchrotron radiation is found to be considerable, and we also demonstrate that our chosen β -functions and emittances are sensitive to the Oide limit. Future mitigation studies to reduce the impact of synchrotron radiation and the Oide effect are discussed, requiring a more careful redesign of the final focusing system. Other plans for the beam delivery system are considered, including the implementation of a round-beam final focusing system utilizing passive plasma lenses, the addition of a collimation section, and the further optimization of higher-order beam aberrations to maximize the luminosity.

-
- [1] K L Brown. A conceptual design of final focus systems for linear colliders. Stanford Linear Accelerator Center, Menlo Park, CA (USA), 06 1987. URL <https://www.osti.gov/biblio/6281389>.
- [2] E R Lindstrom and L S Taylor. Proceedings of the 1987 IEEE particle accelerator conference: Accelerator engineering and technology. None, IEEE Service Center, Piscataway, NJ, 12 1986. URL <https://www.osti.gov/biblio/7189349>.

- [3] D. Burke. Fftb. the final focus test beam project. page p. 283–294., Jun 1993.
- [4] Pantaleo Raimondi and Andrei Seryi. Novel final focus design for future linear colliders. *Phys. Rev. Lett.*, 86:3779–3782, Apr 2001. doi: 10.1103/PhysRevLett.86.3779. URL <https://link.aps.org/doi/10.1103/PhysRevLett.86.3779>.

Focusing Element	K [m^{-2}]	L [mm]	f [cm]
Superconducting Quadrupole: $G = 100$ T/m	0.06	410	4100
Permanent Magnetic Quadrupole: $G = 500$ T/m	0.3	180	1800
Underdense Plasma Lens: $n_0 = 10^{17} \text{cm}^{-3}$	180	7.4	74

TABLE IV: Comparison of different focusing elements for a 5 TeV electron beam assuming a uniform phase advance $\Delta\psi = \sqrt{KL} = 0.1$ across the element.

- [5] G. R. White, R. Ainsworth, T. Akagi, J. Alabau-Gonzalvo, D. Angal-Kalinin, S. Araki, A. Aryshev, S. Bai, P. Bambade, D. R. Bett, G. Blair, C. Blanch, O. Blanco, N. Blaskovic-Kraljevic, B. Bolzon, S. Boogert, P. N. Burrows, G. Christian, L. Corner, M. R. Davis, A. Faus-Golfe, M. Fukuda, J. Gao, H. García-Morales, N. Geffroy, H. Hayano, A. Y. Heo, M. Hildreth, Y. Honda, J. Y. Huang, W. H. Hwang, Y. Iwashita, S. Jang, A. Jeremie, Y. Kamiya, P. Karataev, E. S. Kim, H. S. Kim, S. H. Kim, Y. I. Kim, S. Komamiya, K. Kubo, T. Kume, S. Kuroda, B. Lam, K. Lekomtsev, S. Liu, A. Lyapin, E. Marin, M. Masuzawa, D. McCormick, T. Naito, J. Nelson, L. J. Nevay, T. Okugi, T. Omori, M. Oroku, H. Park, Y. J. Park, C. Perry, J. Pflingstner, N. Phinney, A. Rawankar, Y. Renier, J. Resta-López, M. Ross, T. Sanuki, D. Schulte, A. Seryi, M. Shevelev, H. Shimizu, J. Snuverink, C. Spencer, T. Suehara, R. Sugahara, T. Takahashi, R. Tanaka, T. Tauchi, N. Terunuma, R. Tomás, J. Urakawa, D. Wang, M. Warden, M. Wendt, A. Wolski, M. Woodley, Y. Yamaguchi, T. Yamanaka, J. Yan, K. Yokoya, and F. Zimmermann. Experimental validation of a novel compact focusing scheme for future energy-frontier linear lepton colliders. *Phys. Rev. Lett.*, 112:034802, Jan 2014. doi: 10.1103/PhysRevLett.112.034802. URL <https://link.aps.org/doi/10.1103/PhysRevLett.112.034802>.
- [6] M. Patecki, D. Bett, E. Marin, F. Plassard, R. Tomás, K. Kubo, S. Kuroda, T. Naito, T. Okugi, T. Tauchi, and N. Terunuma. Probing half β_y^* optics in the accelerator test facility 2. *Phys. Rev. Accel. Beams*, 19:101001, Oct 2016. doi: 10.1103/PhysRevAccelBeams.19.101001. URL <https://link.aps.org/doi/10.1103/PhysRevAccelBeams.19.101001>.
- [7] R. Yang, A. Pastushenko, A. Aryshev, M. Bergamaschi, V. Cilento, A. Faus-Golfe, M. Fukuda, P. Korysko, K. Kubo, S. Kuroda, T. Naito, T. Okugi, F. Plassard, N. Terunuma, and R. Tomás. Tuning the ultralow β^* optics at the kek accelerator test facility 2. *Phys. Rev. Accel. Beams*, 23:071003, Jul 2020. doi: 10.1103/PhysRevAccelBeams.23.071003. URL <https://link.aps.org/doi/10.1103/PhysRevAccelBeams.23.071003>.
- [8] R. Yang, A. Pastushenko, V. Cilento, K. Kubo, T. Naito, T. Okugi, N. Terunuma, and R. Tomás. Momentum bandwidth of the kek accelerator test facility 2. *Phys. Rev. Accel. Beams*, 24:051001, May 2021. doi: 10.1103/PhysRevAccelBeams.24.051001. URL <https://link.aps.org/doi/10.1103/PhysRevAccelBeams.24.051001>.
- [9] Rogelio Tomás García, Yuki Yoshi Ohnishi, and Frank Zimmermann. Smallest vertical beam sizes achieved in high-energy accelerators, 2025. URL <https://arxiv.org/abs/2506.12361>.
- [10] Hector García Morales and Rogelio Tomás García. Final-focus systems for multi-TeV linear colliders. *Phys. Rev. ST Accel. Beams*, 17:101001, Oct 2014. doi: 10.1103/PhysRevSTAB.17.101001. URL <https://link.aps.org/doi/10.1103/PhysRevSTAB.17.101001>.
- [11] C. A. Lindstrøm, S. Corde, R. D’Arcy, S. Gessner, M. Gilljohann, M. J. Hogan, and J. Osterhoff. Beam-driven plasma-wakefield acceleration, 2025. URL <https://arxiv.org/abs/2504.05558>.
- [12] Ian Blumenfeld et al. Energy doubling of 42 GeV electrons in a metre-scale plasma wakefield accelerator. *Nature*, 445:741–744, 2007. doi: 10.1038/nature05538.
- [13] M. Litos, E. Adli, W. An, C. I. Clarke, C. E. Clayton, S. Corde, J. P. Delahaye, R. J. England, A. S. Fisher, J. Frederico, S. Gessner, S. Z. Green, M. J. Hogan, C. Joshi, W. Lu, K. A. Marsh, W. B. Mori, P. Muggli, N. Vafaei-Najafabadi, D. Walz, G. White, Z. Wu, V. Yakimenko, and G. Yocky. High-efficiency acceleration of an electron beam in a plasma wakefield accelerator. *Nature (London)*, 515(7525), 11 2014. doi: 10.1038/nature13882.
- [14] G. White, S. Gessner, E. Adli, G.J. Cao, K. Sjobak, S. Barber, C. Schroeder, D. Terzani, J. van Tilborg, E. Esarey, C. Doss, M. Litos, I. Lobach, J. Power, and C.A. Lindstrøm. Beam delivery and final focus systems for multi-TeV advanced linear colliders. *Journal of Instrumentation*, 17(05):P05042, May 2022. ISSN 1748-0221. doi: 10.1088/1748-0221/17/05/p05042. URL <http://dx.doi.org/10.1088/1748-0221/17/05/P05042>.
- [15] Roman Martin, Maria Ilaria Besana, Francesco Cerutti, Andy Langner, Rogelio Tomás, Emilia Cruz-Alaniz, and Barbara Dalena. Interaction region design driven by energy deposition. *Phys. Rev. Accel. Beams*, 20:081005, Aug 2017. doi: 10.1103/PhysRevAccelBeams.20.081005. URL <https://link.aps.org/doi/10.1103/PhysRevAccelBeams.20.081005>.
- [16] Enrico Manosperti, Rogelio Tomás, and Andrii Pastushenko. Design of CLIC beam delivery system at 7 TeV. *JACoW, IPAC2023:MOPL113*, 2023. doi: 10.18429/JACoW-IPAC2023-MOPL113.
- [17] Lewis Kennedy, Conrad Caliani, Vera Cilento, Rogelio Tomás García, and Philip Burrows. Design and performance evaluation of the CLIC beam delivery system at 7 TeV. *submitted to Phys. Rev. Accel. Beams*, December 2025.
- [18] Kaoru Yokoya and Pisin Chen. *Beam-beam phenomena in linear colliders*, page 415–445. Springer Berlin

- Heidelberg. ISBN 9783540467977. doi: 10.1007/3-540-55250-2_37. URL http://dx.doi.org/10.1007/3-540-55250-2_37.
- [19] Spencer Gessner et al. Design Initiative for a 10 TeV pCM Wakefield Collider. 3 2025.
- [20] Helmut Wiedemann. *Particle Accelerator Physics*. Springer Cham, 2015. URL <https://doi.org/10.1007/978-3-319-18317-6>.
- [21] Andrii Pastushenko, Rogelio Tomás, and Angeles Faus-Golfe. Optics design with longer L^* for the final focus system of compact linear collider 380 gev. *Phys. Rev. Accel. Beams*, 26:091003, Sep 2023. doi: 10.1103/PhysRevAccelBeams.26.091003. URL <https://link.aps.org/doi/10.1103/PhysRevAccelBeams.26.091003>.
- [22] Katsunobu Oide. Synchrotron-radiation limit on the focusing of electron beams. *Phys. Rev. Lett.*, 61:1713–1715, Oct 1988. doi: 10.1103/PhysRevLett.61.1713. URL <https://link.aps.org/doi/10.1103/PhysRevLett.61.1713>.
- [23] O. R. Blanco, R. Tomás, and P. Bambade. Beam focusing limitation from synchrotron radiation in two dimensions. *Phys. Rev. Accel. Beams*, 19:021002, Feb 2016. doi: 10.1103/PhysRevAccelBeams.19.021002. URL <https://link.aps.org/doi/10.1103/PhysRevAccelBeams.19.021002>.
- [24] Fabien Plassard, Andrea Latina, Eduardo Marin, Rogelio Tomás, and Philip Bambade. Quadrupole-free detector optics design for the compact linear collider final focus system at 3 tev. *Phys. Rev. Accel. Beams*, 21:011002, Jan 2018. doi: 10.1103/PhysRevAccelBeams.21.011002. URL <https://link.aps.org/doi/10.1103/PhysRevAccelBeams.21.011002>.
- [25] Oscar Blanco, Rogelio Tomas, and Philip Bambade. Oide Effect and Radiation in Bending Magnets. Technical report, CERN, Geneva, 2014. URL <https://cds.cern.ch/record/1967497>.
- [26] Oscar Blanco-García, Philip Bambade, and Rogelio Tomás. Oide Limit Mitigation Studies. page MOPHA004, 2015. URL <https://cds.cern.ch/record/2141800>.
- [27] P. Chen, K. Oide, A. M. Sessler, and S. S. Yu. Plasma-based adiabatic focuser. *Phys. Rev. Lett.*, 64:1231–1234, Mar 1990. doi: 10.1103/PhysRevLett.64.1231. URL <https://link.aps.org/doi/10.1103/PhysRevLett.64.1231>.
- [28] Tim Barklow, Spencer Gessner, Mark Hogan, Cho-Kuen Ng, Michael Peskin, Tor Raubenheimer, Glen White, Erik Adli, Gevy Jiawei Cao, Carl A. Lindstrøm, Kyrre Sjobak, Sam Barber, Cameron Geddes, Arianna Formenti, Remi Lehe, Carl Schroeder, Davide Terzani, Jeroen van Tilborg, Jean-Luc Vay, Edoardo Zoni, Christopher Doss, Michael Litos, Ihar Lobach, John Power, Maximilian Swiatlowski, Luca Fedeli, Henri Vincenti, Thomas Grismayer, Marija Vranic, and Wenlong Zhang. Beam delivery and beamstrahlung considerations for ultra-high energy linear colliders. *Journal of Instrumentation*, 18(09):P09022, sep 2023. doi: 10.1088/1748-0221/18/09/P09022. URL <https://doi.org/10.1088/1748-0221/18/09/P09022>.
- [29] Dongxing He, Arianna Formenti, Spencer Gessner, and Michael Peskin. Analytical approximations for beamstrahlung at very high energy electron-positron colliders, 2025. URL <https://arxiv.org/abs/2511.20912>.
- [30] So Chigusa, Simon Knapen, Toby Opferkuch, Inbar Savoray, Christiane Scherb, and Weishuang Linda Xu. Searches for electroweak states at future plasma wakefield colliders, 2025. URL <https://arxiv.org/abs/2512.09995>.
- [31] R. Tomás. Nonlinear optimization of beam lines. *Phys. Rev. ST Accel. Beams*, 9:081001, Aug 2006. doi: 10.1103/PhysRevSTAB.9.081001. URL <https://link.aps.org/doi/10.1103/PhysRevSTAB.9.081001>.
- [32] H Grote and F Schmidt. MAD-X. 2003. URL <https://cds.cern.ch/record/618496>.
- [33] F Schmidt, E Forest, and E McIntosh. Introduction to the polymorphic tracking code. Technical report, CERN, Geneva, 2002. URL <https://cds.cern.ch/record/573082>.
- [34] D Martinez, A Rosam, R Tomas, and R De Maria. MAP-CLASS2: a code to aid the optimisation of lattice design. 2012. URL <https://cds.cern.ch/record/1491228>.
- [35] Placet. https://abpcomputing.web.cern.ch/codes/codes_pages/Pig.
- [36] Guinea-pig. <https://twiki.cern.ch/twiki/bin/view/ABPComputing/Pig>.
- [37] C. E. Doss, E. Adli, R. Ariniello, J. Cary, S. Corde, B. Hidding, M. J. Hogan, K. Hunt-Stone, C. Joshi, K. A. Marsh, J. B. Rosenzweig, N. Vafaei-Najafabadi, V. Yakimenko, and M. Litos. Laser-ionized, beam-driven, underdense, passive thin plasma lens. *Phys. Rev. Accel. Beams*, 22:111001, Nov 2019. doi: 10.1103/PhysRevAccelBeams.22.111001. URL <https://link.aps.org/doi/10.1103/PhysRevAccelBeams.22.111001>.
- [38] P. Chen, S. Rajagopalan, and J. Rosenzweig. Final focusing and enhanced disruption from an underdense plasma lens in a linear collider. *Phys. Rev. D*, 40:923–926, Aug 1989. doi: 10.1103/PhysRevD.40.923. URL <https://link.aps.org/doi/10.1103/PhysRevD.40.923>.
- [39] P. Manwani, Y. Kang, J. Mann, B. Naranjo, G. Andonian, and J. B. Rosenzweig. Analysis of the blowout plasma wakefields produced by drive beams with elliptical symmetry. *Phys. Rev. Lett.*, 135:095001, Aug 2025. doi: 10.1103/28c4-blhg. URL <https://link.aps.org/doi/10.1103/28c4-blhg>.
- [40] J. S. T. Ng, P. Chen, H. Baldis, P. Bolton, D. Cline, W. Craddock, C. Crawford, F. J. Decker, C. Field, Y. Fukui, V. Kumar, R. Iverson, F. King, R. E. Kirby, K. Nakajima, R. Noble, A. Ogata, P. Raimondi, D. Walz, and A. W. Weidemann. Observation of plasma focusing of a 28.5 gev positron beam. *Physical Review Letters*, 87(24), November 2001. ISSN 1079-7114. doi: 10.1103/physrevlett.87.244801. URL <http://dx.doi.org/10.1103/PhysRevLett.87.244801>.
- [41] P. Muggli, B. E. Blue, C. E. Clayton, F. J. Decker, M. J. Hogan, C. Huang, C. Joshi, T. C. Katsouleas, W. Lu, W. B. Mori, C. L. O’Connell, R. H. Siemann, D. Walz, and M. Zhou. Halo formation and emittance

growth of positron beams in plasmas. *Physical Review Letters*, 101(5), July 2008. ISSN 1079-7114. doi: 10.1103/physrevlett.101.055001. URL <http://dx.doi.org/10.1103/physrevlett.101.055001>.

[org/10.1103/PhysRevLett.101.055001](http://dx.doi.org/10.1103/PhysRevLett.101.055001).